Zn^{2+}-Dependent Misfolding of the p53 DNA Binding Domain

James S. Butler‡ and Stewart N. Loh*

Department of Biochemistry and Molecular Biology, SUNY Upstate Medical University, 750 East Adams Street, Syracuse, New York 13210

Received October 10, 2006; Revised Manuscript Received December 26, 2006

ABSTRACT: The DNA binding domain (DBD) of p53 folds by a complex mechanism that involves parallel pathways and multiple intermediates, both on- and off-pathway. This heterogeneity renders DBD particularly susceptible to misfolding and aggregation. The origins of parallel folding mechanisms are not well understood. DBD folding heterogeneity may be caused by the presence of the single bound Zn^{2+}. To test that hypothesis, we carried out kinetic folding studies of DBD in its Zn^{2+}-free form (apoDBD) and in the presence of various concentrations of free Zn^{2+} and the Zn^{2+}−nitrilotriacetate (NTA) complex. Folding kinetics of apoDBD and DBD are similar, although apoDBD folds faster than DBD at some urea concentrations. The principle consequence of Zn^{2+} removal is to accelerate unfolding and simplify it from two exponential phases to one. Metal binding interactions are therefore not responsible for the observed complexity of the folding reaction. A slight stoichiometric excess of free Zn^{2+} arrests folding and traps the protein in a misfolded state in which Zn^{2+} is bound to nonphysiological ligands. Folding can be rescued by providing metal ions in the form of the NTA−Zn^{2+} complex, which simultaneously protects against misligation and provides a source of Zn^{2+} for regenerating the functional protein. This chemical metallochaperone strategy may be an effective means for improving folding efficiency of other metal binding proteins. The findings suggest that, in vivo, DBD must fold in an environment where free Zn^{2+} concentration is low and its bioavailability is carefully regulated by cellular metallochaperones.

Tumor suppressor p53 is a transcription factor that integrates cellular damage signals and coordinates cell cycle arrest, apoptosis, and/or senescence (*1*). Roughly half of all cancers contain p53 mutations, and almost all of these are located in the DNA binding domain (DBD)[1] (*2*). Previous studies suggest that functional loss results from destabilization of the native state, loss of key DNA contacts, or both (*3*−*6*). We recently proposed a kinetic folding mechanism which accounts for a puzzling observation that is not explained by the destabilization model, namely, that wild-type (WT) DBD spontaneously loses DNA binding function at temperatures where it is thermodynamically stable (*7*). The DBD folding mechanism is unusually complex. It involves multiple kinetic partitioning steps which give rise to parallel folding channels and numerous intermediates, some of which are believed to be misfolded and aggregation prone. Parallel folding mechanisms have been proposed for numerous proteins (*8*−*13*), but, with the exception of proline cis/trans isomerization in the unfolded state (*14*−*19*), the origins of heterogeneity remain largely unknown. Double-jump kinetic experiments (*14*) suggest that proline isomerization is not the source of heterogeneity in the present case (*7*).

Here, we examine the role that metal binding plays in DBD folding. DBD contains a single Zn^{2+} ion coordinated to Cys176 and His179 on the L2 loop and Cys238 and Cys242 on the L3 loop (Figure 1). This interaction maintains the loops in the proper orientation to interact with the minor groove (*3*). We previously determined that removing Zn^{2+} eliminates sequence specificity of DNA binding (*20*). Zn^{2+}-free DBD (apoDBD) is a cooperatively folded protein, although it is less stable and more aggregation prone than DBD. NMR experiments found that the NMR resonances of residues in the L2 and L3 loops shift upon Zn^{2+} removal. In agreement with our results, a recent molecular dynamics study predicted that the structures of apoDBD and DBD are similar except for the region around L2 (*21*).

How might metal or other cofactor binding affect protein folding mechanisms and contribute to heterogeneity? One scenario is that the cofactor may make non-native contacts in unfolded or intermediate states, thereby introducing kinetic traps and hindering productive folding. A well-characterized example of this phenomenon is heme misligation in the unfolded state of cytochrome *c* (*22*). Improper Zn^{2+} binding may be especially problematic for DBD, as it contains 10 Cys (all reduced) and 9 His residues. The second possibility is that cofactors may accelerate folding. If the binding site is formed during the rate-limiting step of folding, then ligand binding will lower the free energy of the transition state, as in the case of Ca^{2+} binding to α-lactalbumin (*23*, *24*). A similar outcome may be achieved if the cofactor makes native contacts in the unfolded state. This interaction may serve to bias the initial conformational search toward native-like structures and thus guide folding down productive pathways.

* To whom correspondence should be addressed. Tel: (315) 464-8731. Fax: (315) 464-8750. E-mail: lohs@upstate.edu.

‡ Present address: Department of Biology, Massachusetts Institute of Technology, 77 Massachusetts Ave., Cambridge, MA 02139.

[1] Abbreviations: apoDBD, DBD with Zn^{2+} ion removed; CD, circular dichroism; DBD, DNA binding domain of human p53 (residues 94−312); DF, direct folding; EMSA, electrophoretic mobility shift assay; IF, interrupted folding; NTA, nitrilotriacetate.

10.1021/bi062106y CCC: $37.00
Published on Web 02/13/2007

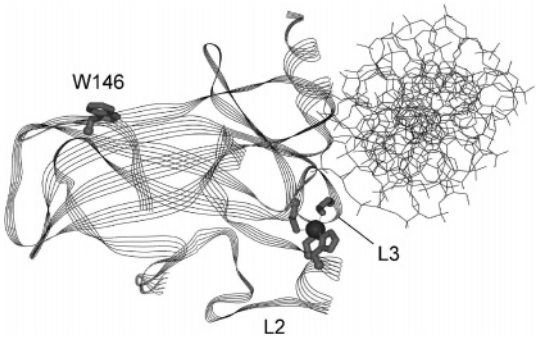

FIGURE 1: X-ray crystal structure of DBD bound to DNA (*3*). The Zn^{2+} ion is shown as a dark gray sphere. Zn^{2+} binding residues, as well as Trp146, are shown in light gray. Loops L2 and L3 are indicated.

Flavin mononucleotide was suggested to facilitate folding of flavodoxin by this mechanism (*25*). The third possibility is that the cofactor may not affect folding rates at all (*26*−*28*). Binding is instead manifested by a slower unfolding rate, indicating that the major binding interactions are present only in the native state.

The extent to which protein−ligand interactions shape the folding landscape is of general interest because a substantial fraction of all proteins require metals or other cofactors to carry out their functions. This issue is particularly important for p53. We previously demonstrated that Zn^{2+} dissociates rapidly from WT DBD at 37 °C and even faster from tumorigenic mutants (*20*). This finding suggests that, in the cell, p53 may refold in the apo form and/or in the presence of a range of Zn^{2+} stoichiometries. Metal concentration must therefore be considered explicitly when formulating folding, misfolding, and inactivation mechanisms of p53.

MATERIALS AND METHODS

Sample Preparation and Spectroscopic Measurements. DBD was expressed and purified as previously described (*7*). ApoDBD was prepared by treating DBD with excess EDTA at pH 4.3, as noted (*20*). Samples were then desalted using a PD-10 column (Amersham) equilibrated with Chelex-treated buffer. To ensure that all 10 Cys residues remained in their native (reduced) form, 2 mM dithiothreitol was present in all buffers during purification. During the final desalting step, dithiothreitol was replaced by tris(2-carboxyethyl)phosphine hydrochloride (TCEP). Cys residues were verified to be fully reduced by assays employing 5,5′-dithiobis(2-nitrobenzoic acid) (not shown). Residual levels of Zn^{2+} were undetectable by assays employing the Zn^{2+}-chelating agent 4-(2-pyridylazo)resorcinol (*29*). Unless otherwise indicated, sample conditions were 0.6−1.0 μM protein, 10 mM 4-(2-hydroxyethyl)-1-piperazineethanesulfonic acid (HEPES) (pH 7.0), 0.10 M NaCl, and 1 mM TCEP. The temperature was 10 °C for all experiments. CD data were collected on a model 202 spectropolarimeter (Aviv Biomedical). Kinetic experiments employed a bandpass setting of 2 nm and a 1 cm path length cuvette with stirring to ensure complete mixing. Steady-state experiments were collected using a 1 mm path length cuvette and 12 μM DBD. Due to significant buffer absorbance below 215 nm, 10 mM sodium phosphate (7.0) was used in place of HEPES. Steady-state and manual mixing kinetic fluorescence experiments were performed on a Fluoromax-3 fluorometer (Jobin-Yvon/SPEX). Excitation and emission were 280 and 355 nm, respectively. All data were collected using 1 cm × 1 cm cuvettes, with stirring, to ensure homogeneity and minimize photobleaching.

DNA Binding Assays. Electrophoretic mobility shift assays (EMSA) employed a 30-mer DNA oligonucleotide bearing the *gadd*45 p53 recognition sequence (four DBD binding sites) (*30*). DNA binding conditions were as noted above with the addition of 5% glycerol, 4.6 μg/mL *gadd*45 oligonucleotide, and 14 μg/mL pBluescript DNA. Free and DBD-bound *gadd*45 were resolved by gel electrophoresis (4% polyacrylamide, 30 mM Tris−borate (pH 7.5), 0.1% Triton X-100, running for 40 m at 100 V on a Bio-Rad Mini-Protean II system, 4 °C). Gels were stained with SYBR Gold (Molecular Probes) and scanned on a Typhoon imager (Amersham). DNA band intensities were quantitated using the Image J software package (NIH). Free *gadd*45 intensities were plotted against total DBD concentration ($[DBD]_T$) and fit to the equation:

$$\text{fraction bound} = ([DBD]_T^{\,n})/([DBD]_T^{\,n} + K_d^{\,n}) \quad (1)$$

where n is the cooperativity parameter (Hill coefficient) and K_d is the DBD/*gadd*45 dissociation constant.

Kinetic Experiments. Zn^{2+}-induced DBD aggregation was monitored by visible light scatter at 500 nm using a Varian Cary-100 spectrophotometer. The DBD concentration was fixed at 2 μM, and the $ZnCl_2$ concentration was varied.

Direct folding (DF) and direct unfolding (DU) experiments were described in detail previously (*7*). Briefly, samples were refolded by the double-jump method (unfold in 7 M urea for 30 s, refold by diluting into buffer) to minimize Pro isomerization in the unfolded state. For DF experiments, folding was monitored directly by Trp fluorescence. Data were fit to one-, two-, or three-exponential functions using the Kaleidagraph software package (Synergy Software). Because track d appears as a missing phase in DF experiments, DF amplitudes are normalized to the sum of the total observed folding amplitude ($A_a + A_b + A_c$).

For IF experiments, the protein was allowed to refold for various times (indicated on the *x*-axes of the figures), whereupon the solution was mixed with urea to a final concentration of 2.8 M (apoDBD) or 4.8 M (DBD). The protein unfolds at these urea concentrations, and the rate and amplitude of the unfolding reaction were recorded by Trp fluorescence. Native DBD and native apoDBD unfold with rates that are distinct from each other and are slower than those of intermediates. The observed unfolding rate therefore reveals which of the two native species is present at the time of unfolding, and the observed amplitude (divided by the corresponding amplitude of a sample that has never been unfolded) indicates the fraction of molecules that have attained that native state. Data were fit to one- and two-exponential functions as described above. IF experiments resolve the amplitude of track d (but not the rate); this value is reported in the text. Final urea concentrations were determined by measuring refractive indices of each sample at the end of the experiment (*31*).

For DF and IF experiments carried out in the presence of Zn^{2+} and chelators, these compounds were not present when the protein was unfolded. Rather, they were added to the refolding buffer prior to folding.

Scheme 1: DBD Folding Mechanism (Left) and Schematic Representation of Fast- and Slow-Folding Channels (Right)[a]

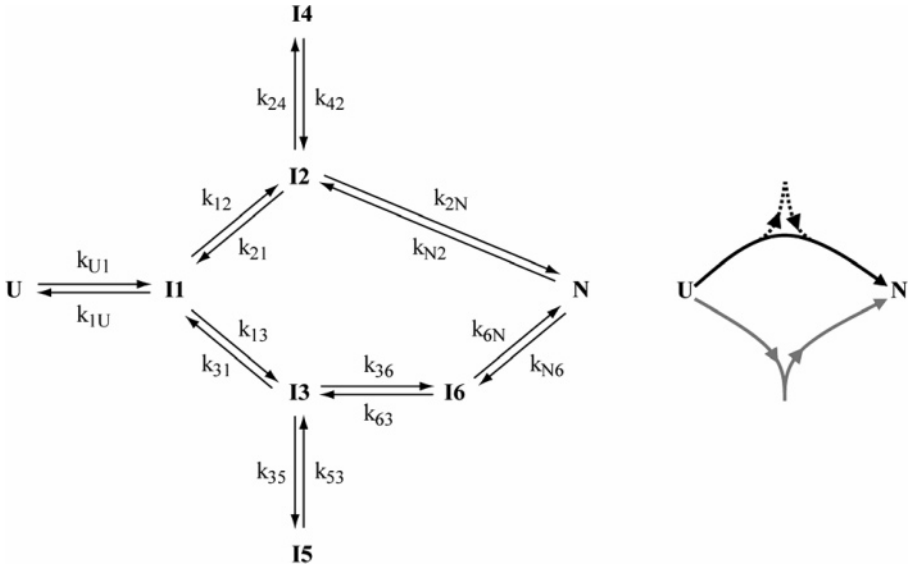

[a] The fast and slow channels are the upper and lower pathways, respectively, on the left and are colored black and gray on the right. Folding tracks are depicted in the right panel as follows: track a, solid black line; track b, solid black and dashed black lines; track c, gray line. Track d is not shown. Microscopic rate constants that reproduce $k_{obs,a}$, $k_{obs,b}$, and $k_{obs,c}$ and their associated amplitudes in the absence of denaturant (10 °C) are as follows (in units of s^{-1}): $k_{U1} = 200$, $k_{1U} = 30$, $k_{12} = 1$, $k_{21} = 0.001$, $k_{13} = 0.4$, $k_{31} = 0.01$, $k_{24} = 0.04$, $k_{42} = 0.02$, $k_{35} = 0.1$, $k_{53} = 0.02$, $k_{2N} = 0.08$, $k_{N2} = 1 \times 10^{-5}$, $k_{36} = 0.001$, $k_{63} = 8 \times 10^{-7}$, $k_{6N} = 0.3$, and $k_{N6} = 0.005$.

RESULTS

DBD Folding Mechanism. We first present a brief overview of the DBD folding mechanism (Scheme 1). DBD folds through two main channels, designated fast and slow. The channels are set by a kinetic partitioning event that is established early in folding. Partitioning occurs when the two forward rate constants (k_{12} and k_{13} in this instance) are comparable, and the reverse rate constants (k_{21} and k_{31}) are slower than the subsequent forward rate constants. Molecules are thus committed to remain in each pathway once the initial choice is made. The fast channel (upper pathway in Scheme 1) is in turn comprised of two tracks, which are generated by another partitioning step at intermediate I2. A subset of molecules fold directly to N (track a), and the remaining portion misfolds to the dead-end species I4 (track b). Thus, the fast channel is comprised of track a and track b. Track a represents the fastest route to the native state. In order for molecules in track b to rejoin the productive folding stream, I4 must unfold to I2. Evidence for this step comes from the unusual observation that the track b refolding rate increases with denaturant concentration from 0 to 1.4 M urea (*7*).

Of the molecules that partition into the slow channel (lower pathway in Scheme 1), nearly all pass through dead-end intermediate I5 (because $k_{35} \gg k_{36}$). The slow channel is therefore comprised of a single track (track c), which follows the sequence U−I1−(I3/I5)−I6−N. I6 is not observed in refolding experiments, presumably because it lies on the other side of the transition state. It is placed in the mechanism to account for the biphasic unfolding kinetics observed for DBD at 10 °C (*7*). The fourth track, track d, is very slow and appears as a "missing" phase in refolding experiments. It is not shown in Scheme 1. We do not characterize it further, although we have established by double-jump experiments that it is most likely not caused by proline isomerization in the unfolded state. In summary, DBD folds by four tracks whose rates differ by several orders of magnitude. At one extreme, track a is complete in ∼30 s; at the other, track d requires ∼10 h.

The fraction of molecules that partition into each track is remarkably constant. For WT DBD at 10 °C, approximately one-fourth of molecules fold by each of the four tracks. This ratio holds true for temperatures up to 35 °C and for tumorigenic mutants G245S, R249S, and R282Q (*32*). The folding mechanism, although complex and indicative of both on- and off-pathway intermediates, is nevertheless robust and reproducible in different conditions and for a variety of mutants.

Zn^{2+} Binding to Native and Unfolded States. Fluorescence and CD spectra of DBD and apoDBD are unique. Though subtle, apoDBD fluorescence emission is more quenched than that of DBD from 300 to 325 nm (Figure 2A). CD spectra reveal greater changes: Zn^{2+} loss results in more negative ellipticity at wavelengths above ∼205 nm (Figure 2B). We therefore used the change in CD ellipticity at 230 nm to monitor the rate of Zn^{2+} loss from DBD. DBD (12 μM) was incubated in the presence of a 20-fold excess of EDTA at 10 °C. Ten percent and 46% of Zn^{2+} dissociate in 24 and 72 h, respectively (not shown), indicating that the dissociation rate constant is roughly 1×10^{-6}−2×10^{-6} s^{-1}. This value is comparable to the unfolding rates measured at 10 °C ($k_{obs,a}{}^{unf} = 1 \times 10^{-5}$ s^{-1}; $k_{obs,b}{}^{unf} = 8 \times 10^{-7}$ s^{-1}) (*7*), suggesting that Zn^{2+} dissociation is limited by global unfolding. Consistent with this idea is the observation that Zn^{2+} dissociates within minutes at 37 °C, which is again similar to the DBD unfolding rate at this temperature (unfolding is monophasic at 37 °C) (*20*, *32*).

In contrast to native DBD, Zn^{2+} dissociates from unfolded DBD within seconds. This rapidity allowed us to measure the Zn^{2+} binding affinity in 6 M urea. Urea-denatured DBD is known to bind Zn^{2+} with submicromolar affinity (*4*, *20*), although the dissociation constant (K_d) has not been reported. Using a competition assay with the fluorescent chelator

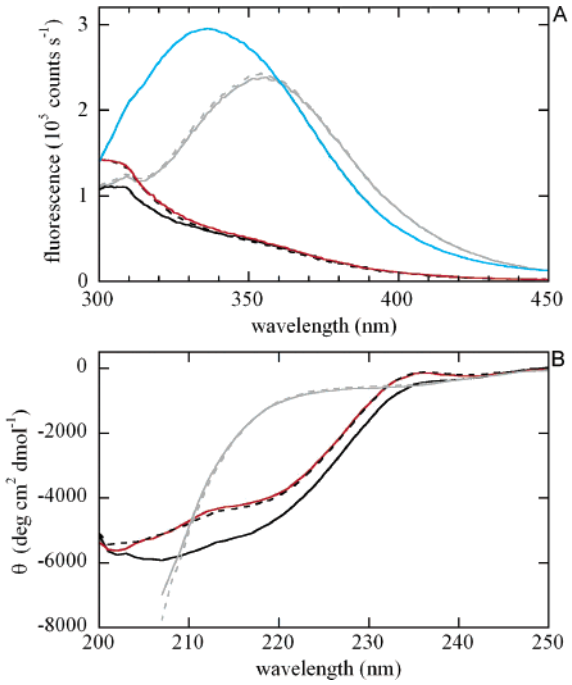

FIGURE 2: (A) Fluorescence spectra of native apoDBD (solid black), native DBD (dashed black), unfolded apoDBD (solid gray), unfolded DBD (dashed gray), aggregated DBD (DBD + 30 μM $ZnCl_2$; blue), and reconstituted DBD (apoDBD + 75 μM NTA−30 μM $ZnCl_2$; red). The protein concentration is 4 μM, and unfolded samples are in 6 M urea. (B) CD spectra of native apoDBD (solid black), native DBD (dashed black), unfolded apoDBD (solid gray), unfolded DBD (dashed gray), and reconstituted DBD (apoDBD + 140 μM NTA−54 μM $ZnCl_2$; red). The protein concentration is 12 μM, and unfolded samples are in 6 M urea.

Indo-1 (*33*), we find that K_d = 1.0 nM in 6 M urea (Supporting Information, Figure S1). The relatively high affinity of this interaction raises the possibility that some residual structure may be present in the unfolded state. However, fluorescence and CD spectra of apoDBD and DBD are identical in 6 M urea (Figure 2), indicating that residual structure, if present, is not extensive. DBD contains 10 Cys residues, which are all in their reduced form and are thus potential ligands for metal binding. To test whether Cys residues are responsible for Zn^{2+} binding in the unfolded state, we blocked the thiol groups with methyl methanethiosulfonate. K_d increased by over 100-fold (data not shown). Unfolded DBD thus binds Zn^{2+} via thiol groups, although whether by native or non-native Cys residues remains unknown. Importantly, these results confirm that DBD folding initiates from the fully Zn^{2+}-bound state under our experimental conditions.

ApoDBD Folding and Unfolding. To address the effects of Zn^{2+} on DBD folding, we first carried out direct folding (DF) and interrupted folding (IF) experiments on apoDBD. DF monitors the decrease in fluorescence of Trp146 as the protein, initially unfolded in 7 M urea, is induced to refold by mixing with buffer. IF adds a second mixing step in which the refolding protein is transferred back into 2.8 M urea (apoDBD) or 4.8 M urea (DBD). The unfolding reaction is then followed by Trp fluorescence. Native molecules unfold with a characteristic (slow) rate, whereas intermediates unfold faster (typically in the mixing dead time). Thus, the fraction of native molecules formed at the time of the unfolding pulse can be deduced from the amplitude of the unfolding reaction.

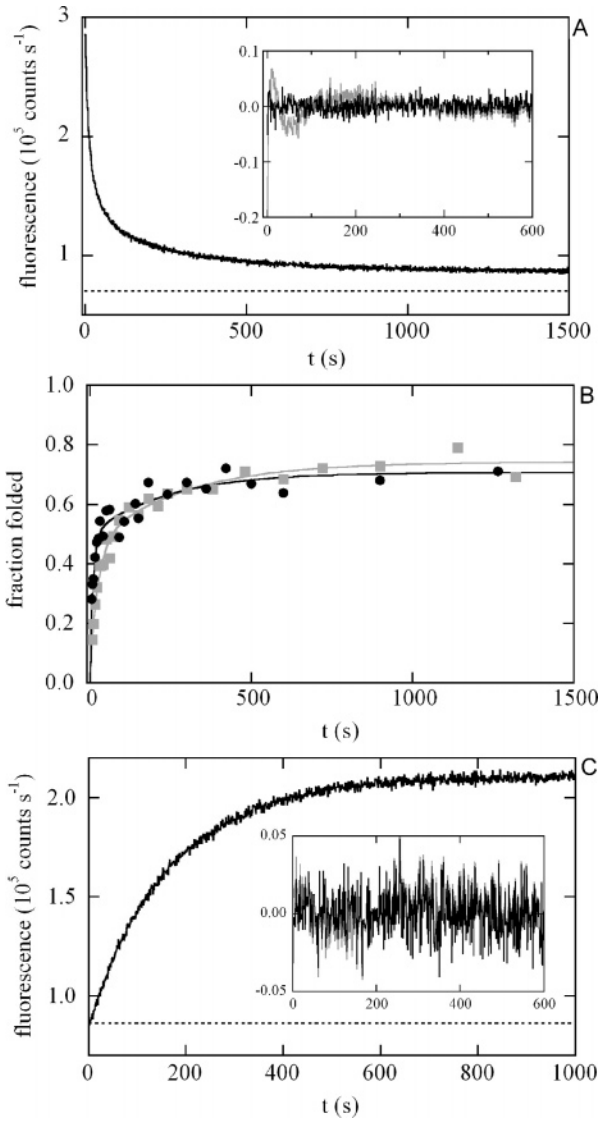

FIGURE 3: (A) DF kinetics of apoDBD monitored by Trp fluorescence (0.6 μM apoDBD, 0.3 M urea). The dashed line is the native baseline. The solid line indicates the best fit to a three-exponential function. The inset shows residuals to two-exponential (gray line) and three-exponential (black line) fits. Units of the inset are the same as those of the plot. (B) IF kinetics of apoDBD (black circles) and DBD (gray squares). The refolding buffer contains 0.3 M urea. Lines are best fits of the data to two-exponential functions (see text). DBD data are taken from ref *7*. (C) Direct unfolding kinetics of apoDBD in 2.4 M urea monitored by Trp fluorescence. The dashed line is the extrapolated native baseline. The inset shows residuals from one-exponential (gray line) and two-exponential (black line) fits. Units of the inset are the same as those of the plot.

In both DF and IF experiments, apoDBD is unfolded by a double-jump sequence to minimize Pro isomerization in the unfolded state.

In low denaturant concentrations, apoDBD folds in a manner very similar to that of DBD. Stopped-flow DF experiments (Supporting Information, Figure S2) detect a submillisecond burst-phase increase in fluorescence, corresponding to formation of I1. Fluorescence then decays with a minimum of three exponential phases (indicative of tracks a−c) whose rates and amplitudes are nearly identical to those of DBD (Figure 3A, Table 1). A fourth phase (track d) requires ~10 h to complete and consequently appears as a missing amplitude (cf. dashed line in Figure 3A).

Table 1: DF and IF Kinetic Parameters for ApoDBD and DBD in 0.3 M Urea and in 1.0 M Urea[a]

	DF (0.3 M urea)		IF (0.3 M urea)		IF (1.0 M urea)		
	apoDBD	DBD	apoDBD	DBD	apoDBD	apoDBD + NTA−Zn^{2+}	DBD
$k_{obs,a}$ (s^{-1})	0.11	0.090	NR[b]	NR	NR	NR	NR
$k_{obs,b}$ (s^{-1})	0.011	0.014	NR	NR	NR	NR	NR
$k_{obs,c}$ (s^{-1})	0.0025	0.0022	0.0051	0.0036	0.0079	0.0059	0.0027
A_a (%)	43	44	49[c]	45[c]	77[c]	82[c]	48[c]
A_b (%)	31	30	49[c]	45[c]	77[c]	82[c]	48[c]
A_c (%)	26	26	20	29	15	8.1	40
A_d (%)	ND[d]	ND	31	26	8	10	12

[a] Uncertainties are estimated to be 10% and 20% of the reported DF and IF values, respectively, based on error analysis of multiple data sets. [b] NR, not resolved. Curve fit did not resolve $k_{obs,a}$ from $k_{obs,a}$ due to the increased mixing dead time of IF experiments. [c] Sum of A_a and A_b (see text). [d] ND, not determined.

We next performed IF experiments to monitor formation of native apoDBD molecules in 0.3 M urea. IF data are minimally fit by a burst phase, followed by a two-exponential increase and then a slow, unresolved phase (Figure 3B). Native molecules are therefore formed by at least four processes. The burst phase likely corresponds to formation of N via track a. The burst phase and the faster of the two observable phases are not well resolved in IF, because the dead time and data sampling interval are longer than in DF. As a result, individual values of $k_{obs,a}$ and $k_{obs,b}$ cannot be determined accurately. The sum of A_a and A_b, however, is well determined by the sum of the burst-phase amplitude and the amplitude of the fast phase. Given this consideration and the close agreement of the primary data, IF data for apoDBD and DBD are in reasonable accord. IF additionally reveals that ~30% of molecules fold through the very slow pathway (track d) in 0.3 M urea.

In contrast to refolding, Zn^{2+} binding has a pronounced effect on unfolding. ApoDBD unfolding data fit well to a single-exponential function yielding an unfolding rate (k_{obs}^{unf}) of 0.0059 s^{-1} in 2.4 M urea (Figure 3C). Extrapolation of the native baseline indicates that the observed phase accounts for the entire unfolding amplitude (data not shown), indicating that no unresolved phases are present. On the other hand, DBD unfolding is biphasic at all urea concentrations examined (*7*). The unfolding rate of apoDBD is significantly faster than either of the two DBD unfolding rates when compared at the same urea concentration.

To characterize the stabilities of kinetic intermediates and their rates of formation, which dictate flux through each folding track, we measured folding and unfolding kinetics of apoDBD at various urea concentrations. The resulting chevron plots of rates and amplitudes are shown in panels A and B of Figure 4, respectively. The noteworthy features of Figure 4A are the dual-chevron curves, suggesting parallel pathways, and the inverse rollover between 0 and 1.4 M urea that argues for misfolded intermediates in the slower two of the three refolding limbs. These characteristics are present for both apoDBD and DBD. The apoDBD chevron has a minimum at 2.0 M urea. This value is the same as the midpoint of urea denaturation (C_m) measured by equilibrium experiments and reflects the lower stability of apoDBD relative to DBD (C_m = 2.8 M urea) (*20*).

We previously determined that amplitudes of the refolding phases obtained by DF and IF experiments are within 10% of each other at all urea concentrations tested (*7*). This equivalence indicates that DF amplitudes can be used to estimate the fraction of native molecules that fold by each

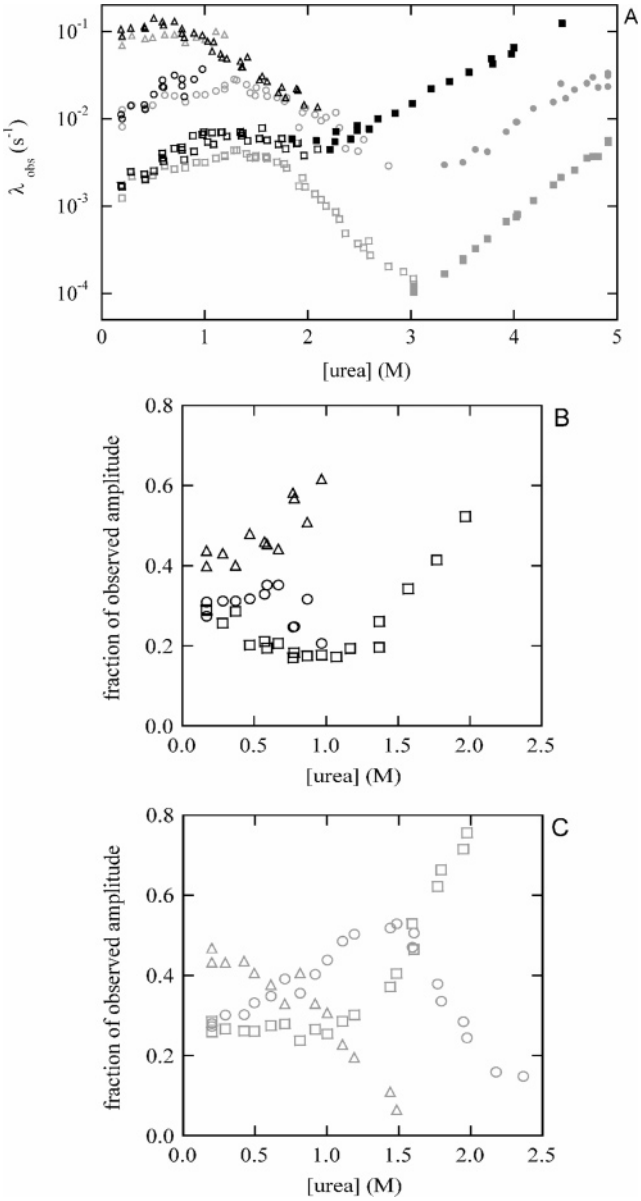

FIGURE 4: (A) Urea dependence of observed folding (open symbols) and unfolding (closed symbols) rates of apoDBD (black) and DBD (gray), obtained from DF and direct unfolding experiments. Symbols are as follows: triangles, $k_{obs,a}$; circles, $k_{obs,b}$; squares, $k_{obs,c}$. (B) Urea dependence of observed folding amplitudes of apoDBD. Symbols are as follows: triangles, A_a; circles, A_b; squares, A_c. (C) Urea dependence of observed folding amplitudes of DBD. Symbols are the same as in panel B. DBD data are taken from ref *7*.

track. In the absence of denaturant, approximately equal fractions of apoDBD fold via track a, track b, and track c

(Figure 4B). As urea concentration increases, molecules partition into track a at the expense of track b. This shift is likely caused by I4 becoming unstable. Since I4 is a kinetic trap, a greater percentage of molecules that pass through the fast channel fold directly to N (via track a). Surprisingly, the opposite trend was observed for DBD (Figure 4C). In 1.0 M urea, ~60% of apoDBD folds by track a whereas this figure is only ~30% for DBD. This difference engenders two predictions: (i) apoDBD should fold faster than DBD at ~1 M urea; (ii) formation of functional molecules can be made more efficient by refolding the protein in the apo form (in 1 M urea) and then introducing Zn^{2+} once the native state is attained. We test these hypotheses in the next section.

Effect of Zn^{2+} Availability on DBD Folding. The absence of Zn^{2+} does not adversely affect folding and can accelerate it at moderately low urea concentrations. Excess Zn^{2+}, however, is highly deleterious to the folding reaction. Figure 5A depicts folding of apoDBD when $ZnCl_2$ is present in the refolding buffer. Folding is inhibited by as low as a 2-fold excess of $ZnCl_2$ and is nearly abolished by a 4-fold excess. Figure 5B shows that DBD folding, completely arrested by a 20-fold excess of $ZnCl_2$, can be rescued by addition of metal chelators [EDTA, EGTA, and nitrilotriacetate (NTA)]. A straightforward explanation for this behavior is that Zn^{2+} coordinates to non-native sites when the apoDBD is in intermediate states, trapping the protein in misfolded conformations. Misligation can be to groups within a single protein or shared between two or more molecules. The latter interaction appears to occur in native DBD. Visible aggregation is observed after addition of $ZnCl_2$ in as little as a 2:1 molar ratio and becomes more pronounced with increasing $ZnCl_2$ concentrations (Figure 5C).

Figure 5B suggests a metallochaperone strategy for enhancing the rate and yield of DBD refolding. The idea is to use a compound that binds Zn^{2+} with greater affinity than the putative non-native site(s), but with lower affinity than the native site. The protein can then fold in the apo form, which offers an efficient route to the native state (especially in moderate urea concentrations). ApoDBD abstracts metal from the chelator only after the high-affinity site is formed in the native state. The compound thus serves as both a sink and a source of zinc ions, depending on the state of the protein. Another requirement is that the dissociation rate of the chelator$-Zn^{2+}$ complex should be relatively rapid ($\geq 10^{-2}$ s^{-1}), so that the functional DNA binding form can be generated quickly. Assuming a diffusion-limited on-rate of 10^8 $M^{-1}\cdot s^{-1}$, K_d should thus be greater than $\sim 10^{-10}$ M. EDTA binds Zn^{2+} too tightly to be an effective Zn^{2+} source [$K_d = 8.1 \times 10^{-14}$ M at pH 7.0, 0.1 M NaCl, 10 °C, calculated using the WEBMAXC program (http://www.stanford.edu/~cpatton/webmaxc/) which is based on stability constants of Martell and Smith (*34*)]. We therefore chose NTA ($K_d = 1.7 \times 10^{-8}$ M).

As an initial test, we mixed native apoDBD (4 μM) with NTA (75 μM) and $ZnCl_2$ (30 μM). Fluorescence and CD spectra reveal that apoDBD abstracts Zn^{2+} from NTA to generate DBD (Figure 2). Without NTA, 30 μM $ZnCl_2$ causes DBD to aggregate visibly within minutes (Figure 5C). Prior to the onset of turbidity, a large increase in Trp fluorescence is observed with a maximum near 340 nm (Figure 2A). This spectrum has been attributed to a soluble aggregated form of DBD which can be generated by heating

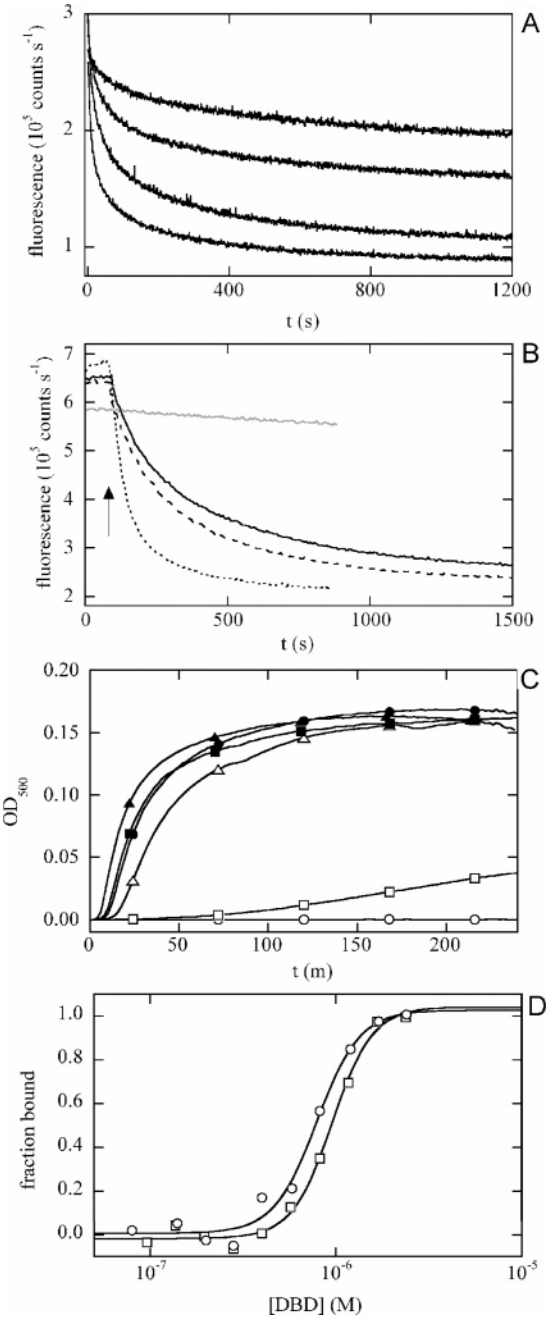

FIGURE 5: (A) Inhibition of apoDBD folding by free Zn^{2+} monitored by Trp fluorescence. $ZnCl_2$ was either absent (lowest trace) or present in the refolding buffer at 1.2, 1.8, and 2.4 μM concentrations (upper traces, from low to high). The apoDBD concentration is 0.6 μM. (B) Rescue of DBD folding by metal chelators. DBD (0.75 μM) was refolded in the presence of 16 μM $ZnCl_2$. After 80 s of stalled folding (indicated by the arrow), NTA (solid line), EGTA (long dashes), EDTA (short dashes), or nothing (gray line) was added to the solution. The chelator concentration is 0.5 mM. (C) $ZnCl_2$-induced aggregation of native DBD monitored by light scatter at 500 nm. $ZnCl_2$ concentrations are 4 μM (open squares), 10 μM (open triangles), 14 μM (closed circles), 18 μM (closed squares), 40 μM (closed triangles). DBD does not aggregate in the presence of 74 μM $ZnCl_2$ and 186 μM NTA (open circles). (D) Sequence-specific DNA binding affinity of DBD (circles) and apoDBD reconstituted with 75 μM NTA$-$30 μM $ZnCl_2$ DBD (squares), determined by EMSA. Lines indicate best fits of the data to eq 1. Fitted parameters are $K_d = 0.79$ μM, $n = 3.8$ (DBD) and $K_d = 0.95$ μM, $n = 4.0$ (reconstituted apoDBD).

the protein at 37 °C or higher (*4*, *35*). Importantly, in the presence of a 2.5-fold excess of NTA, Zn^{2+}-induced ag-

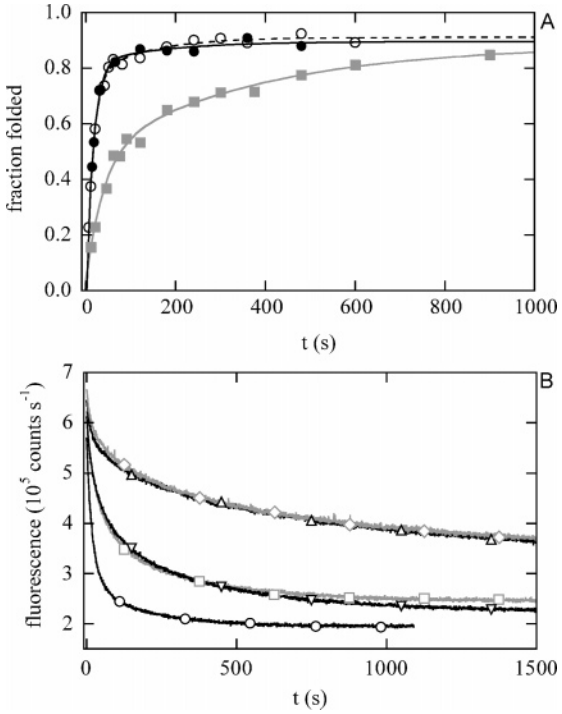

FIGURE 6: (A) Formation of native molecules in 1.0 M urea determined by IF. Symbols are as follows: gray squares, DBD; open circles (dashed line), apoDBD; closed circles (solid line), DBD generated by refolding apoDBD and adding NTA−$ZnCl_2$ immediately prior to the unfolding pulse (see text). Lines are best fits of the data to a two-exponential function. (B) NTA rescue of Zn^{2+}-dependent misligation monitored by DF. Symbols are as follows: circles, apoDBD; gray squares, DBD; gray diamonds, DBD + 62 μM NTA−25 μM $ZnCl_2$; triangles, DBD + 15 μM NTA−6 μM $ZnCl_2$; inverted triangles, DBD + 125 μM NTA−6 μM $ZnCl_2$. The protein concentration is 1.0 μM, and the urea concentration is 1.0 M.

gregation is not detected either by fluorescence (Figure 2A) or by light scatter (Figure 5C). In fact, further raising $ZnCl_2$ and NTA concentrations to 74 and 186 μM, respectively, does not induce aggregation (Figure 5C). ApoDBD binds Zn^{2+} in the mixing dead time, indicating that the metal dissociates from NTA within seconds. To determine whether the reconstituted protein is active, we performed electrophoretic mobility shift assays (EMSA) using a DNA oligonucleotide bearing the *gadd*45 recognition sequence (*20*). Refolded DBD binds the oligonucleotide with similar affinity and cooperativity as DBD that had not been unfolded or exposed to NTA−$ZnCl_2$ (Figure 5D). Together, these data demonstrate that not only does NTA protect native DBD from Zn^{2+}-induced aggregation, it is an effective source of metal ions for regenerating the functional protein.

Panels B and C of Figure 4 suggest that, at moderate urea concentrations, removing bound Zn^{2+} causes a greater percentage of molecules to fold via the fastest track (track a). Moreover, Figures 2 and 5C establish that the NTA−$ZnCl_2$ complex rapidly introduces Zn^{2+} to native apoDBD. These results imply that a particularly efficient method to generate functional DBD is to refold the protein in its apo form in 1 M urea and then add the NTA−Zn^{2+} complex to native apoDBD. To test the first part of that hypothesis, we carried out IF experiments in 1 M urea. As predicted, apoDBD folds significantly faster than DBD (Figure 6A, Table 1). For example, at 50 s of folding, 48% of DBD molecules have reached the native state; that figure is 80% for apoDBD (an increase of 67%). To test the second part of the hypothesis, we performed the same experiment except NTA−$ZnCl_2$ (150 μM/60 μM) was added immediately prior to the last unfolding pulse (final urea concentration of 4.8 M). An advantage of this method is that apoDBD and DBD can be distinguished by their markedly different unfolding rates: apoDBD unfolds in the mixing dead time in 4.8 M urea (Figure 4A). When apoDBD is refolded in this manner, it unfolds with the same, slow rate as the DBD control (data not shown), indicating that DBD reconstitution is complete within the mixing dead time (<5 s). Figure 6A demonstrates that formation of active DBD can be accelerated by folding through the Zn^{2+}-free state and then regenerating the Zn^{2+}-bound protein by NTA-mediated metal ion transfer.

Can NTA protect DBD from Zn^{2+} misligation that occurs during the folding reaction? To answer that question, we refolded DBD by dilution into buffer that contained various NTA−$ZnCl_2$ concentrations. Figure 5B established that 16 μM $ZnCl_2$ completely halts folding. Using the same 2.5:1 (NTA−$ZnCl_2$) ratio employed in the previous experiments, we find that 62 μM NTA allows DBD to fold in the presence of 25 μM $ZnCl_2$, albeit at a reduced rate (Figure 6B). NTA thus protects against misligation, but not completely. There are two explanations for the observed inhibition. First, it could be caused by the presence of free Zn^{2+} that is not bound by NTA. Figure 5A indicates that $[Zn^{2+}]_{free}$ must be at least 2-fold greater than [DBD] for appreciable inhibition to be observed. This scenario is improbable, as $[Zn^{2+}]_{free}$ (calculated to be 5×10^{-9} M) is only 0.5% of the total protein concentration. The likely explanation is that inhibition is caused by Zn^{2+} partitioning from NTA into non-native binding sites on DBD. No such abstraction is detected once DBD has attained the native conformation (Figures 2 and 5C,D). These findings indicate that the non-native sites (i) are formed early in the folding process, (ii) bind Zn^{2+} more tightly than NTA, and (iii) are not present in the native state. In other words, DBD is especially vulnerable to Zn^{2+}-induced misfolding when in intermediate conformations.

To further test the ability of NTA to rescue folding, we refolded DBD in the presence of 6 μM Zn^{2+} and either 15 or 125 μM NTA. In the absence of NTA, 6 μM $ZnCl_2$ is expected to block folding (Figure 5A). Folding is partially restored by 15 μM NTA and is fully rescued by 125 μM NTA (Figure 6B). Folding in the presence of a strong chelator such as EDTA might seem to produce the same effect as NTA but at lower chelator concentrations. The product of that reaction, however, would likely be apoDBD. Available evidence suggests that Zn^{2+} binds to EDTA more tightly than to DBD at 37 °C (*20*). Furthermore, the dissociation rate of the EDTA−Zn^{2+} complex, estimated to be $\sim 10^{-5}$ s^{-1}, is too slow to generate functional protein in a biologically relevant time scale.

DISCUSSION

Effect of Zn^{2+} on DBD Folding. There are two main findings of this study. The first is that heterogeneity of the DBD folding reaction is not caused by metal binding. ApoDBD folds via four tracks which, in the absence of denaturant, are characterized by kinetic rates and amplitudes similar to those of DBD. Thus, heterogeneity is an intrinsic property of the DBD folding landscape. The second is that

kinetic traps can play a dominant role in DBD folding. Some traps are caused by improper Zn^{2+} binding, while others are inherent to the DBD sequence and occur whether Zn^{2+} is present or not. I4 and I5 are examples of the latter. These off-pathway intermediates are populated during folding of both apoDBD and DBD at low urea concentrations. Zn^{2+} removal, however, appears to destabilize I4 so that it melts out near 1 M urea. As a result, the flux of refolding molecules shifts from track b to track a in a cooperative manner with increasing urea (Figure 4B). Above 1 M urea, partitioning is broken, and molecules that entered the fast channel fold exclusively via track a.

The presence of Zn^{2+}-dependent kinetic barriers is demonstrated clearly by Figure 5A,B. A 20-fold excess of Zn^{2+} traps the protein in one or more highly fluorescent intermediate states. The barrier to resolution is high, as evidenced by the fact that folding is essentially blocked until a large excess of chelator is added. The intermediate ensemble binds Zn^{2+} in the presence of a 62-fold excess of NTA (Figure 6B), suggesting subnanomolar affinity. It is interesting to note that these binding sites are not present after DBD has attained the native state. Folded apoDBD appears to abstract only a single metal ion from the pool of NTA−Zn^{2+}. This ion is bound by native ligands and restores proper DNA binding function (Figure 5D). Misfolded forms are not detected by fluorescence (Figure 2A) or CD (Figure 2B) spectra. Metal misligation sites are indeed present on folded DBD, as shown by Figure 5C, but they are of relatively weak affinity and cannot compete with NTA for Zn^{2+} binding.

Why do high-affinity, non-native Zn^{2+} binding sites exist in intermediate but not native states? Tight binding requires four ligands arranged in tetrahedral geometry. Within a single native molecule, the only combination of Cys and His side chains capable of providing that positioning are the natural Zn^{2+} binding residues. Since free Zn^{2+} causes native DBD to aggregate visibly, it is likely that misligation in the folded form arises from metal ions coordinating side chains from different protein molecules. Intermolecular binding is expected to be weaker than intramolecular binding, consistent with NTA competition experiments. In contrast, when Zn^{2+} is present in the refolding buffer, it arrests folding without the lag phase or turbidity associated with aggregation. Intermediates thus appear to bind metal ions in an intramolecular fashion. We propose that the flexibility and lack of structure of folding intermediates allow them to sample conformations that expose at least one non-native, high-affinity metal binding site, i.e., where one (or more) of the four side chains is not a physiological ligand.

Metal misligation is limited to Zn^{2+} and Cd^{2+}. Divalent cations Ca^{2+}, Fe^{2+}, Mg^{2+}, Mn^{2+}, Co^{2+}, and Ni^{2+} do not interfere with folding at molar ratios of 20:1 (data not shown). Nor do these ions induce aggregation of native DBD. In fact, Co^{2+}, and to a lesser extent Ni^{2+}, appears to bind native apoDBD and restore the CD spectrum of DBD (not shown). Cd^{2+} is known to bind in the Zn^{2+} site and inactivate p53 (*36*). Consistent with that result, we find that Cd^{2+} and Zn^{2+} have nearly identical effects on DBD folding and aggregation (not shown). The transient metal binding sites in DBD folding intermediates therefore appear to retain the specificity of the physiological site.

Having characterized some of the major kinetic traps in DBD folding, we were able to identify conditions which minimize these pitfalls. First, removing Zn^{2+} altogether ensures that metal misligation cannot occur. Second, the combination of Zn^{2+} removal and 1 M urea destabilizes the dead-end intermediate I4 and allows more molecules to fold via track a. Third, providing metal ions in the form of the NTA−Zn^{2+} complex regenerates DBD rapidly, while simultaneously protecting it from Zn^{2+}-induced aggregation. The result is that functional DBD can be formed more quickly than by refolding the natural 1:1 protein−Zn^{2+} complex (Figure 6A).

The stabilizing effect of metal binding is manifested primarily as a decreased unfolding rate rather than an increased folding rate. This finding indicates that the native Zn^{2+} binding pocket is not formed in the major transition state. Thus, although at least one non-native binding site is created within the mixing time of refolding experiments, the physiological site is made in the final stage of folding. Another effect of Zn^{2+} removal is that it changes unfolding from a biphasic to a monophasic reaction. Scheme 1 attributes biexponential kinetics to accumulation of I6. We previously found that the tumorigenic mutants G245S and R249S exhibit monophasic unfolding in their Zn^{2+}-bound forms (*7*). We speculated that these mutations may destabilize I6 and cause it to be depopulated (*7*). Gly245 and Arg249 are located in the L3 loop that contributes two ligands to Zn^{2+}. Removal of Zn^{2+} may exert a localized effect similar to that of the mutations. In support of this notion, the R282Q mutation, which lies outside of the Zn^{2+}-binding region, destabilizes DBD to the same extent as R249S but displays biphasic unfolding (although with faster rates than WT DBD) (*7*).

Physiological Importance of Zn^{2+} Bioavailability. Our results emphasize the critical importance of intracellular metal ion regulation to p53 function in vivo. At micromolar DBD concentrations, more than a 2-fold excess of free Zn^{2+} inhibits or arrests folding (Figure 5A). If Zn^{2+} is removed altogether, then apoDBD folds without risk of misligation. Native apoDBD, however, aggregates quickly in a Zn^{2+}-independent fashion (*20*). Moreover, apoDBD unfolds faster than DBD and hence undergoes more unfolding−folding cycles per unit time. We previously argued that the longevity of DBD is correlated with unfolding rate, because a fraction of molecules is effectively trapped in nonfunctional states with each cycle (most likely due to aggregation of I4 and I5) (*7*). Metal ions must be supplied quickly, to regenerate functional DBD before these misfolding events can occur. The final complication is that free Zn^{2+} itself induces aggregation of DBD, when present in as low as a 2-fold molar excess (Figure 5C).

How does the cell resolve this conundrum? With total intracellular Zn^{2+} levels as high as 1 mM (*37*), the concentration of free Zn^{2+} is thought to be held in the 10 pM range by binding to proteins and other chelators in the cell (*38*). This study identifies some of the characteristics that a chelator should possess in order for it to be an effective metallochaperone for DBD. It should bind Zn^{2+} tightly enough, or be present in sufficient abundance, so that the free Zn^{2+} concentration is below K_d of the misligation interaction (estimated to be $<10^{-9}$ M). It should also release metal ions fast enough to deliver it to the physiological binding site in a timely manner. These conditions would seem to place strict limits on strength of the chelator−Zn^{2+}

interaction. They can, however, be tempered by adjusting the total concentrations and ratios of chelator and Zn^{2+}. For example, thionein (the metal-free form of metallothionein) inactivates p53 in vitro (*39*). In contrast, moderate overexpression of metallothionein significantly enhances p53 activity in vivo, probably by serving as a Zn^{2+} source. More extensive overexpression of metallothionein once again inhibits p53 activity. Similarly, Zn^{2+} deficiency results in elevated p53 expression but reduced activity in rat glioma cells (*40*). These results underscore the importance of balancing the metallochaperone:Zn^{2+} ratio.

The experiments in this study were performed with WT DBD at 10 °C. Zn^{2+} affinity of native DBD decreases with increasing temperature and in the presence of tumorigenic mutations (*20*). This trend may favor misligation if temperature and mutation destabilize the native state to a greater extent than intermediate forms, as available evidence indicates (*32*). Our findings demonstrate that improper Zn^{2+} binding can inhibit or block DBD folding and suggest that this may represent a significant inactivation pathway for mutant p53 in the cell. Regulation of intracellular Zn^{2+} levels is likely to be a critical aspect of maintaining proper p53 function.

ACKNOWLEDGMENT

We thank Dr. Jeung-Hoi Ha for discussions and for critical review of the manuscript.

SUPPORTING INFORMATION AVAILABLE

Figures showing the determination of Zn^{2+} binding affinity of unfolded DBD (Figure S1) and DF kinetics of apoDBD monitored by stopped-flow fluorescence (Figure S2). This material is available free of charge via the Internet at http://pubs.acs.org.

REFERENCES

1. Vogelstein, B., Lane, D., and Levine, A. J. (2000) Surfing the p53 network, *Nature 408*, 307−310.
2. Olivier, M., Eeles, R., Hollstein, M., Khan, M. A., Harris, C. C., and Hainault, P. (2002) The IARC TP53 database: new online mutation analysis and recommendations to users, *Hum. Mutat. 19*, 607−614.
3. Cho, Y., Gorina, S., Jeffrey, P. D., and Pavletich, N. P. (1994) Crystal structure of a p53 tumor suppressor-DNA complex: Understanding tumorigenic mutations, *Science 265*, 346−355.
4. Bullock, A. N., Henckel, J., DeDecker, B. S., Johnson, C. M., Nikolova, P. V., Proctor, M. R., Lane, D. P., and Fersht, A. R. (1997) Thermodynamic stability of wild-type and mutant p53 core domain, *Proc. Natl. Acad. Sci. U.S.A. 94*, 14338−14342.
5. Bullock, A. N., Henckel, J., and Fersht, A. R. (2000) Quantitative analysis of residual folding and DNA binding in mutant p53 core domain: definition of mutant states for rescue in cancer therapy, *Oncogene 19*, 1245−1256.
6. Wong, K.-B., DeDecker, B. S., Freund, S. M., Proctor, M. R., Bycroft, M., and Fersht, A. R. (1999) Hot-spot mutants of p53 core domain evince characteristic local structural changes, *Proc. Natl. Acad. Sci. U.S.A. 96*, 8438−8442.
7. Butler, J. S., and Loh, S. N. (2005) Kinetic partitioning during folding of the p53 DNA binding domain, *J. Mol. Biol. 350*, 906−918.
8. Borgia, A., Bonivento, D., Travaglini-Allocatelli, C., Di Matteo, A., and Brunori, M. (2006) Unveiling a hidden folding intermediate in *c*-type cytochromes by protein engineering, *J. Biol. Chem. 281*, 9331−9336.
9. Pocanschi, C. L., Apell, H. J., Puntervoll, P., Hogh, B., Jensen, H. B., Welte, W., and Kleinschmidt, J. H. (2006) The major outer membrane protein of Fusobacterium nucleatum (FomA) folds and inserts into lipid bilayers via parallel folding pathways, *J. Mol. Biol. 355*, 548−561.
10. Wildegger, G., and Kiefhaber, T. (1997) Three-state model for lysozyme folding: triangular folding mechanism with an energetically trapped intermediate, *J. Mol. Biol. 270*, 294−304.
11. Wright, C. F., Lindorff-Larsen, K., Randles, L. G., and Clarke, J. (2003) Parallel protein-unfolding pathways revealed and mapped, *Nat. Struct. Biol. 10*, 658−662.
12. Krantz, B., and Sosnick, T. R. (2001) Engineered metal binding sites map the heterogeneous folding landscape of a coiled coil, *Nat. Struct. Biol. 8*, 1042−1047.
13. Wallace, L. A., and Matthews, C. R. (2002) Sequential vs. parallel protein-folding mechanisms: experimental tests for complex folding reactions, *Biophys. Chem. 101*−*102*, 113−131.
14. Brandts, J. F., Halvorson, H. R., and Brennan, M. (1975) Consideration of the possibility that the slow step in protein denaturation reactions is due to cis-trans isomerism of proline residues, *Biochemistry 14*, 4953−4963.
15. Kiefhaber, T., Grunert, H. P., Hahn, U., and Schmid, F. X. (1990) Replacement of a cis proline simplifies the mechanism of ribonuclease T1 folding, *Biochemistry 35*, 1548−1559.
16. Schultz, D. A., Schmid, F. X., and Baldwin, R. L. (1992) Cis proline mutants of ribonuclease A. II. Elimination of the slow-folding forms by mutation, *Protein Sci. 1*, 917−924.
17. Wedermeyer, W. J., Welker, E., and Scheraga, H. A. (2002) Proline cis-trans isomerization and protein folding, *Biochemistry 451*, 14637−14644.
18. Maki, K., Ikura, T., Hayano, T., Takahashi, N., and Kuwajima, K. (1999) Effects of proline mutations on the folding of staphylococcal nuclease, *Biochemistry 38*, 2213−2223.
19. Wu, Y., and Matthews, C. R. (2003) Proline replacements and the simplification of the complex, parallel channel folding mechanism for the alpha subunit fo Trp synthase, a TIM barrel protein, *J. Mol. Biol. 330*, 1131−1144.
20. Butler, J. S., and Loh, S. N. (2003) Structure, function, and aggregation of the zinc-free form of the p53 DNA binding domain, *Biochemistry 42*, 2396−2403.
21. Duan, J., and Nilsson, L. (2006) Effects of Zn^{2+} on DNA recognition and stability of the p53 DNA binding domain, *Biochemistry 45*, 7483−7492.
22. Colón, W., Wakem, L. P., Sherman, F., and Roder, H. (1997) Identification of the predominant non-native histidine ligand in unfolded cytochrome *c*, *Biochemistry 36*, 12535−12541.
23. Kuwajima, K., Mitani, M., and Sugai, S. (1989) Characterization of the critical state in protein folding: effects of guanidine hydrochloride and specific Ca^{2+} binding on the folding kinetics of α-lactalbumin, *J. Mol. Biol. 206*, 547−561.
24. Bushmarina, N. A., Blanchet, C. E., Vernier, G., and Forge, V. (2006) Cofactor effects on the protein folding reaction: acceleration of α-lactalbumin refolding by metal ions, *Protein Sci. 15*, 659−671.
25. Apiyo, D., and Wittung-Stafshede, P. (2002) Presence of the cofactor speeds up folding of *Desulfovibrio desulfuricans* flavodoxin, *Protein Sci. 11*, 1129−1135.
26. Sugawara, T., Kuwajima, K., and Sugai, S. (1991) Folding of staphylococcal nuclease A studied by equilibrium and kinetic circular dichroism spectra, *Biochemistry 30*, 2698−2706.
27. Pozdnyakova, I., and Wittung-Stafshede, P. (2001) Copper stabilizes azurin by decreasing the unfolding rate, *Arch. Biochem. Biophys. 290*, 146−148.
28. Goedken, E. R., Keck, J. L., Berger, J. M., and Marqusee, S. (2000) Divalent metal cofactor binding in the kinetic folding trajectory of *Escherichia coli* ribonuclease H1, *Protein Sci. 9*, 1914−1921.
29. Hunt, J. B., Neece, S. H., and Ginsburg, A. (1985) The use of 4-(2-pyridylazo)resorcinol in studies of zinc release from *Escherichia coli* aspartate transcarbamoylase, *Anal. Biochem. 146*, 150−157.
30. Nicholls, C. D., McLure, K. G., Shields, M. A., and Lee, P. (2002) Biogenesis of p53 involves cotranslational dimerization of monomers and posttranslational dimerization of dimers. Implications on the dominant negative effect, *J. Biol. Chem. 277*, 12937−12945.
31. Pace, C. N., and Scholtz, J. M. (1997) *Protein Structure: a Pratical Approach* (Creighton, T. E., Ed.) pp 299−320, Oxford University Press, New York.
32. Butler, J. S., and Loh, S. N. (2006) Folding and misfolding mechanisms of the p53 DNA binding domain at physiological temperature, *Protein Sci.* (in press).

33. Jefferson, J. R., Hunt, J. B., and Ginsburg, A. (1990) Characterization of Indo-1 and Quin-2 as spectroscopic probes for Zn^{2+}-protein interactions, *Anal. Biochem. 187*, 328−336.
34. Martell, A. E., and Smith, R. M. (1974−1989) *Critical Stability Constants*, Vol. 1−6, Plenum Press, New York.
35. Friedler, A., Veprintsev, D. B., Hansson, L. O., and Fersht, A. R. (2003) Kinetic instability of p53 core domain mutants, *J. Biol. Chem. 278*, 24108−24112.
36. Meplan, C., Mann, K., and Hainaut, P. (1999) Cadmium induces conformational modifications of wild-type p53 and supresses p53 response to DNA damage in cultured cells, *J. Biol. Chem. 274*, 31663−31670.
37. Sensi, S. L., Canzoniero, L. M., Yu, S. P., Ying, H. S., Koh, J. Y., Kerchner, G. A., and Choi, D. W. (1997) Measurement of intracellular free zinc in living cortical neurons: routes of entry, *J. Neurosci. 17*, 9554−9564.
38. Simons, T. J. B. (1991) Intracellular free zinc and zinc buffering in human red blood cells, *J. Membr. Biol. 123*, 63−71.
39. Meplan, C., Richard, M.-J., and Hainaut, P. (2000) Metallogregulation of the tumor supressor protein p53: zinc mediates the renaturation of p53 after exposure to metal chelators in vitro and in intact cells, *Oncogene 19*, 5227−5236.
40. Ho, E., and Ames, B. N. (2002) Low intracellular zinc induces oxidative DNA damage, disrupts p53, NFkB, and AP1 DNA binding, and affects DNA repair in a rat glioma cell line, *Proc. Natl. Acad. Sci. U.S.A. 99*, 16770−16775.

BI062106Y